The effective nuclear delivery of doxorubicin from dextran-coated gold nanoparticles larger than nuclear pores

Hongje Jang [b], Soo-Ryoon Ryoo [a], Kostas Kostarelos [c], Sang Woo Han [b,d,**], Dal-Hee Min [a,*]

[a] Institute for Basic Science, Department of Chemistry, Seoul National University, Seoul 151-742, Republic of Korea
[b] Department of Chemistry and KI for the NanoCentury, KAIST, Daejeon 305-701, Republic of Korea
[c] Nanomedicine Lab, Centre for Drug Delivery Research, UCL School of Pharmacy, University College London, London WC1N 1AX, UK
[d] Center for Nanomaterials and Chemical Reactions, Institute for Basic Science, Daejeon 305-701, Republic of Korea

ABSTRACT

To date, gold nanoparticles (AuNPs) have been investigated for diverse bioapplications. Generally, AuNPs are engineered to possess surface coating with organic/inorganic shells to increase colloidal stability in biological solutions and to facilitate chemical conjugation. In the present study, we developed a strategy to prepare dextran-coated AuNPs with control over its size by simply boiling an aqueous solution of Au salt and dextran, in which dextran serves as both reducing agent for AuNP (Au(0)) formation from Au(III) and AuNP surface coating material. The prepared dextran-coated AuNPs (dAuNPs) maintained its colloidal stability under high temperature, high salt concentration, and extreme pH. Importantly, the dAuNP remarkably improved efficacy of an anti-cancer agent, doxorubicin (Dox), when harnessed as a Dox delivery carrier. The half-maximal inhibitory concentration (EC50) of Dox-conjugated dAuNP with diameter of 170 nm was ~9 pM in HeLa cells, which was 1.1×10^5 times lower than that of free Dox and lower than any previously reported values of Dox-nanoparticle complex. Interestingly, smaller AuNPs with 30 and 70 nm showed about 10 times higher EC50 than 170 nm AuNPs when treated to HeLa cells after conjugation with Dox. To achieve high cytotoxicity as cancer therapeutics, Dox should be delivered into nucleus to intercalate with DNA double helix. We show here that Dox-AuNPs was far more efficient as an anti-cancer drug than free Dox by releasing from AuNPs through spontaneous degradation of dextran, allowing free diffusion and nuclear uptake of Dox. We also revealed that larger AuNPs with lower degree of dextran crosslinking promoted faster degradation of dextran shells.

© 2013 Elsevier Ltd. All rights reserved.

1. Introduction

Many strategies for targeted drug delivery to disease sites and tissues have been developed to enhance drug efficacy and reduce side effects [1–7]. Most of them focus on the selective cellular uptake of drug-loaded carriers by abnormal cells, for example, cancer cells [8–11]. Generally, intracellular localization of nanoparticles showed accumulation mostly in the cytoplasm but hardly in nuclei [12–15]. In fact, nuclear transport of nanoparticles is challenging since the nuclear pores have a specific diameter of 30–40 nm and the diffusion rate through such small size pores is greatly dependent on the nanoparticle size [16]. However, nuclear targeting and transport through the nuclear pore complex are important, especially in order to enhance the efficacy of anti-cancer agents such as doxorubicin (Dox), because their cytotoxic activity depends on its intercalation with DNA and subsequent inhibition of topoisomerase II to block DNA replication inside the nucleus [17]. Therefore, the development of drug delivery platforms with the capacity to translocate drugs to the nucleus is important. Ideal drug delivery system (DDS) should keep anti-cancer agents chemically intact and present long-circulation time until they are delivered into the target cells and its nucleus. For this purpose, several nanoparticle-based systems including silica nanoparticles and quantum dots have been developed with nuclear transport capability by conjugation of nuclear localization signals (NLS) [18–22]. For intranuclear uptake of NLS-drug-nanoparticle complex and for achieving high efficacy, the size of nanoparticles has been restricted below ~30–40 nm, smaller than nuclear pores, which limits types of applicable nanoparticles.

Here, we report the synthesis of dextran-coated gold nanoparticles (dAuNPs) for efficient nuclear delivery of Dox, achieved without any NLS (Scheme 1). Gold nanoparticle (AuNP) is one of the
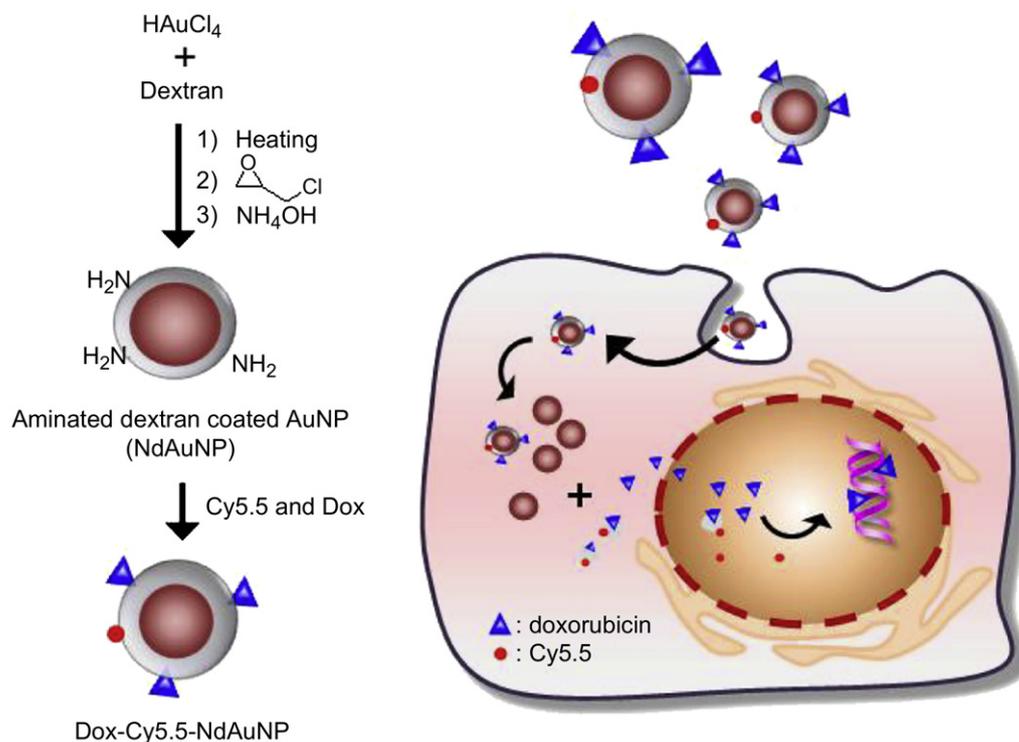
Scheme 1. Synthesis of dextran-coated AuNPs and subsequent conjugation of Cy5.5 and doxorubicin. Dextran plays roles as a reducing agent and a coating material for the AuNPs at the same time. Size of the NdAuNPs can be easily tuned by varying ratio of gold salt to dextran. Bio-degradable dextran coating of the AuNPs might be easily broken into pieces to release doxorubicin from AuNP cores and therefore, diffusion and accumulation of doxorubicin into nucleus could be feasible regardless of the size of original AuNPs.

nanoparticles that have been actively studied in biomedical research in recent years [23,24]. Unique properties including fluorescence quenching [25,26], surface plasmon resonance [27] and relatively low cytotoxicity expedited its application in wide range of researches, demonstrated in immunostaining [28], single particle tracking [29], contrast agents for TEM and X-ray [30,31], vehicle for drug delivery [32,33], hyperthermia [34] and optical trigger [35]. Chemically modified dextrans have been used for Dox delivery. For example, dextran nanoparticles were synthesized by disulfide bond mediated crosslinking and Dox was encapsulated inside the dextran particles [36] and acetal-dextran was self-assembled and stabilized by living radical polymerization [37]. These approaches harnessed dextran only as matrix and Dox was loaded non-covalently during particle preparation. In our strategy, dextran served as a biodegradable polymer that constitutes the shells of the metallic nanoparticle, AuNPs, allowing the release of the covalently-conjugated Dox. The released Dox can then freely diffuse through nuclear pores and accumulate into the nucleus to achieve high apoptotic activity regardless of the size of parent AuNPs. In the present synthesis of the dAuNPs, dextran, a non-cytotoxic carbohydrate polymer, plays roles as a reducing agent for gold nanoparticle core formation and a surface coating for generated gold cores as well [38,39]. We previously reported that the dAuNPs with diameter of ∼80 nm exhibit superb biocompatibility and colloidal stability even under harsh conditions such as high temperature, high salt concentrations and extreme pH [40]. In the present study, the dAuNPs were prepared with three different sizes of 30, 70 and 170 nm in diameter by varying relative concentration of gold salt to dextran. We then investigated colloidal stability, biocompatibility and most importantly, efficiency as a Dox delivery vehicle for anti-cancer agents. We hypothesized that although nuclear delivery of the whole Dox–dAuNP complex larger than nuclear pore (30–40 nm) was hardly possible, Dox–dAuNPs could release Dox from AuNPs through spontaneous degradation

of dextran, allowing free diffusion of Dox from cytoplasm into nucleus after cellular uptake of Dox–dAuNPs. We also investigated that degradation kinetics of dextran shell could be tuned by varying the size of AuNPs and controlling the degree of dextran crosslinking.

2. Materials and methods

2.1. Materials

Hydrogen tetrachloroaurate(III) hydrate was purchased from Kojima Chemicals Co. (Sayama, Saitama, Japan). Ammonium hydroxide (28–30% in H_2O), Dithiothreitol (DTT, 99%), and 3-(4,5-dimethylthiazol-2-yl)-2,5-diphynyl tetrazolium bromide (MTT) were purchased from Sigma (St.Louis, MO, USA). Dextran from leuconostoc ssp. (Mr ∼ 15,000–25,000) was purchased from Fluka. (Milwaukee, WI, USA). Epichlorohydrin (99%) and doxorubicin were purchased from Aldrich (Milwaukee, WI, USA). Sodium hydroxide and trisodium citrate dehydrate were purchased from Junsei (Tokyo, Japan). N-Succinimidyl-3-(2-pyridyldithio)propionate (SPDP), di(N-succinimidyl) glutarate (DSG) and cyanine 5.5 (Cy5.5) were purchased from Pierce (Rockford, IL, USA). DAPI was purchased Vector Laboratories (CA, USA). 10× Phosphate-buffered saline (PBS), Dulbecco's modified eagle's medium (DMEM), and fetal bovine serum (FBS) were purchased from WelGENE (Seoul, Korea). Amicon ultra centrifuge filter devices (cutoff:100 kDa) were purchased from Millipore (Billerica, MA, USA). Minisart RC25 syringe filters (0.20 μm and 0.45 μm pore size) were purchased from Sartorius stedim biotech (Goettingen, Germany). All Chemicals were used as received.

2.2. Synthesis of 30, 70, and 170 nm sized dAuNPs

Dextran (12.0 g) was dissolved in distilled water (160 mL) to prepare 7.5 wt% solution. The solution was heated until boiling and 216, 432 or 864 μL of hydrogen tetrachloroaurate(III) hydrate stock solution (0.1 g/mL) was added to make 30, 70 or 170 nm dAuNP, respectively. The reaction mixture was boiled for ∼20 min until the colors of the mixtures turned deep-violet (30 nm)/reddish-violet (70 nm)/turbid-orange (170 nm). The reaction mixture was then cooled to room temperature. The product was rinsed with distilled water for 4 times using Amicon filter (cutoff: 100 kDa). The product was further purified by passing the mixtures through 0.45 μm and 0.20 μm pore size syringe filter. Finally, dAuNPs were re-dispersed in 4 mL distilled water, and stored at 4 °C.

2.3. Crosslinking of dAuNPs

The 200 (for 30 and 70 nm dAuNPs) or 100 (for 170 nm dAuNPs) μL of 1 M NaOH solution was added to the synthesized 4 mL of dAuNPs. We reduced amount of NaOH for 170 nm dAuNPs to maintain colloidal stability during the reaction. The reaction mixture was vortexed vigorously for 10 s and then, 100 μL of epichlorohydrin was added to the mixture to make 2.5 v/v% mixture. Mixed solution was allowed to incubate with shaking at 1000 rpm on a horizontal shaker overnight at room temperature. Purification of the crosslinked-dAuNPs was performed by centrifugation at 3000 rpm for 20 min using 100 kDa cutoff Amicon ultra centrifuge filter. The product was rinsed with distilled water for 4 times and re-dispersed in 4 mL of distilled water and stored at 4 °C.

2.4. Amination of dAuNPs

Amination was achieved by addition of ammonium hydroxide (3 v/v%, except otherwise indicated) to the aqueous crosslinked-dAuNP solution. Mixed solution was allowed to incubate at room temperature for 24 h at 600 rpm on a horizontal shaker. Purification was carried out by centrifugation at 3000 rpm for 20 min with 100 kDa cutoff Amicon ultra centrifuge filter. The product was rinsed with distilled water for 4 times, and re-dispersed in distilled water. The NdAuNPs remained stable more than 3 months at 4 °C.

2.5. Synthesis of 30, 80 and, 150 nm citrate stabilized AuNPs

The 50 mL of 0.25 mM hydrogen tetrachloroaurate(III) solution was heated to boil and 780 (30 nm)/200 (80 nm)/80 (150 nm) μL of 34 mM trisodium citrate dehydrate solution was then added. The reaction mixtures were boiled for 20 min until the color changed to red (30 nm)/violet (80 nm)/pale violet (150 nm) and then cooled to room temperature.

2.6. Characterization of synthesized NdAuNPs

Field emission SEM XL30SFEG (Philips, USA) and Field emission TEM Tecnai G2 F30 (FEI, Netherlands) were used to obtain images of AuNPs. Particle size distribution was determined by a particle size analyzer Plus90 (Brookhaven). SpectraMax Plus384 (Molecular Devices, USA) was used to obtain UV–Vis absorption spectra. Zeta potential measurement was carried out by a zeta sizer Nano ZS90 (Malvern, UK). Cellular images were collected using a Ti inverted fluorescence microscope equipped with a 60× (1.4 numerical aperture) objective (Nikon Co., Japan) and a CoolSNAP cf charge-coupled device (CCD) camera (Photometrics, Tucson, AZ).

2.7. Conjugation of fluorescent dye to NdAuNPs

To conjugate Cy5.5 fluorescent dye to NdAuNPs, 3 eq. of NHS-Cy5.5 relative to concentration of the nanoparticles in anhydrous DMSO stock solution was added to 30, 70, and 170 nm NdAuNPs in PBS buffer on ice bath. Mixed solutions were allowed to incubate for 24 h at room temperature with shaking at 600 rpm. The fluorescent dye labeled NdAuNPs were purified by centrifugation at 3000 rpm with 100 kDa cutoff Amicon ultra centrifuge filter. The product was rinsed 4 times with distilled water and re-dispersed in distilled water. The number of conjugated Cy5.5 dye molecule per NdAuNPs was estimated by UV-Vis spectrophotometry based on Beer's law ($\varepsilon_{Cy5.5, 675 nm}$: 250,000 L mol^{-1} cm^{-1}).

2.8. Conjugation of doxorubicin to Cy5.5–NdAuNPs

For conjugation of doxorubicin to Cy5.5–NdAuNPs, 100 eq. of di(N-succinimidyl) glutarate (DSG) in anhydrous DMSO relative to concentration of the nanoparticles was added to the Cy5.5–NdAuNPs. Mixed solutions were allowed to incubate for 30 min at room temperature with shaking at 600 rpm and then, 10 eq. of doxorubicin in distilled water was added to mixtures. Further shaking for 3 h at 600 rpm was allowed for conjugation of doxorubicin. Purification was performed by using 100 kDa cutoff Amicon ultra centrifuge filter at 3000 rpm for 20 min. The product was rinsed 4 times with distilled water, and re-dispersed in distilled water. The conjugation ratio of Dox/NP was determined based on Beer's law. ($\varepsilon_{Dox, 480 nm}$: 11,500 L mol^{-1} cm^{-1}).

2.9. Cell culture

HeLa (human cervical cancer) cells were maintained in Dulbecco's Modified Eagle's Medium (DMEM) containing 4.5 g/L D-glucose and supplemented with 10% FBS (fetal bovine serum), 100 units/mL penicillin, and 100 μg/mL streptomycin. The cells were grown in a humidified 5% CO$_2$ incubator at 37 °C.

2.10. MTT assay for viability test

MTT (3-(4,5-dimethylthiazol-2-yl)-2,5-diphenyl tetrazolium bromide) powder was dissolved in 1× PBS at 5 mg/mL concentrations, and filtered by a 0.2 μm pore sized sterilized syringe filter. The stock solution was stored at 4 °C. HeLa cells were seeded with a density of 10,000 cells per well of a 96-well culture plate with 100 μL of growth media (about 50–70% confluency). After Dox–Cy5.5–NdAuNPs and Cy5.5-NdAuNPs with various concentrations were added and incubated for 24 h at 37 °C, cells were rinsed with PBS. A 20 μL MTT stock solution was added to detect the metabolically active cells in each well. The cells were incubated for 2–4 h until purple color developed. The media were discarded, and 200 μL DMSO was added to each well to make water-insoluble formazan salt solubilized. Then, the optical densities of each well in the plates were read at 560 nm. Mean and standard deviation for triplicates were calculated.

2.11. Fluorescence microscopy

HeLa cells were seeded on sterile round-shaped coverslips in 12-well plates at a density of 6×10^4 cells per well and allowed to achieve stable adherence for 24 h. Then, free doxorubicin and doxorubicin conjugated each nanoparticle formulation ([Dox] = 83 pM) were treated to the cells. After incubation for 12 h at 37 °C, the supernatant was carefully removed and the cells were washed with PBS two times. Subsequently, the cells were fixed in 4% paraformaldehyde in PBS (pH 7.4) for 20 min at room temperature. After fixation, cells were washed with PBS three times. Each sample was mounted on a glass slide using mounting medium containing DAPI and observed by using a Ti inverted fluorescence microscope equipped with a 60× objective (1.4 numerical aperture, Nikon Co., Japan) and a CoolSNAP cf charge-coupled device (CCD) camera (Photometrics, Tucson, AZ) with Metamorph image analysis software (Molecular Devices, Sunnyvale, CA, USA).

3. Results and discussion

The dAuNPs of three different sizes were first synthesized by following the previously reported method with modification [40]. Briefly, aqueous solutions of hydrochloroauric acid with various concentrations (0.337, 0.675 and 1.35 mM) were added to a boiling, aqueous dextran solution (7.5 wt%) and each mixture was allowed to boil with stirring until the solution showed turbid reddish colors. After rinsing the mixtures with distilled water, crosslinking and amination reaction were carried out by addition of epichlorohydrin in basic pH condition and ammonium hydroxide. The prepared aminated dAuNPs with different sizes (NdAuNPs, where N stands for amine groups) were characterized by dynamic light scattering (DLS), UV–Vis spectroscopy, transmission electron microscopy (TEM) and scanning electron microscopy (SEM). The hydrodynamic diameters of NdAuNPs measured by DLS were 29.6 ± 1.4, 71.2 ± 7.8 and 169.4 ± 51.6 nm (Fig. 1a, For convenience, each group of NdAuNP was referred as NdAuNP of 30 nm, 70 nm and 170 nm throughout the present paper.). The UV–Vis absorption spectra of the NdAuNPs in distilled water exhibit the red shift of characteristic plasmon bands with increase of the nanoparticle size as expected (Fig. 1b). Diameters estimated from TEM and SEM were similar to the DLS diameter (Fig. 1c).

We next characterized the NdAuNPs by zeta potential and pyridine-2-thione assay (P2T assay). First, zeta potential of the dAuNPs was measured as −3.08, −4.64 and −7.51 mV for 30, 70 and 170 nm dAuNP, respectively. After crosslinking and amination of each dAuNP by using 3 v/v% of NH$_4$OH, zeta potential increased to −0.76, −1.58 and −2.45 mV for NdAuNP of 30, 70 and 170 nm, respectively. Zeta potential of NdAuNP increased as the concentration of ammonium hydroxide increased, indicating that the degree of amination could be tuned by varying the concentration of ammonium hydroxide (Fig. 1d). Next, we quantitatively determined amount of primary amine functional groups by P2T assay [41,42]. P2T assay is a simple spectrophotometric method for the quantitative measurement of amine groups on solid supports, in which excess succinimidyl-3-(2-pyridyldithio)propionate (SPDP) was first treated to the amine-presenting NdAuNPs and, followed by spectroscopic measurement of the amount of released P2T by a reducing agent, dithiothreitol, at 343 nm (extinction coefficient of P2T, $\varepsilon_{P2T, 343 nm} = 8080$ M^{-1} cm^{-1}). Number of the introduced amine groups in the NdAuNPs after the treatment of 3 v/v% ammonium hydroxide was calculated as 2.99×10^5, 5.33×10^5 and 6.74×10^5 per particle for 30, 70 and 170 nm NdAuNP, respectively (Fig. 1e). No
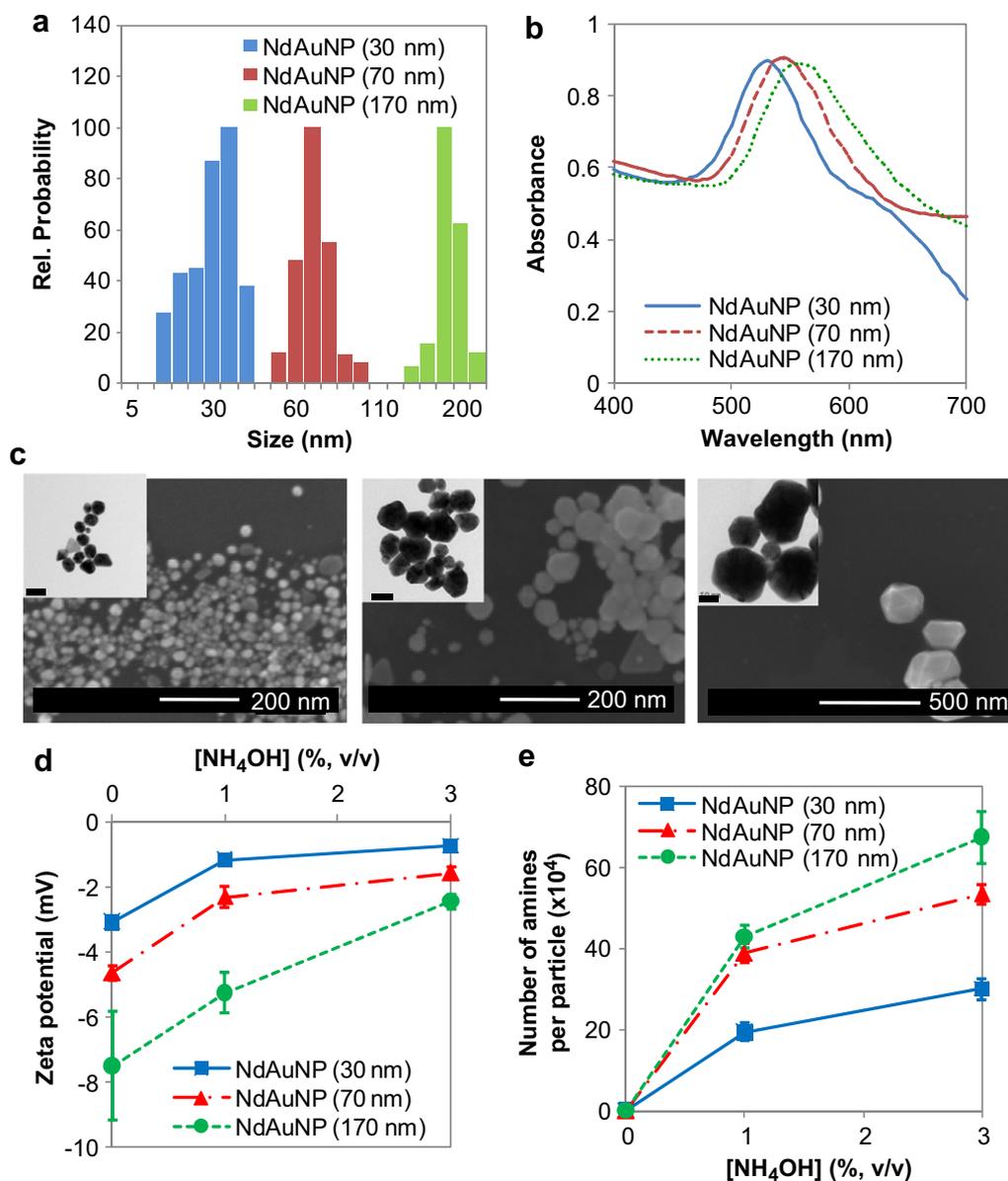
Fig. 1. Characterization of the synthesized aminated dextran-coated AuNPs (NdAuNPs) by DLS, UV−Vis spectroscopy, TEM and SEM. (a) The DLS measurement represented different size distribution of average 29.6 ± 1.4, 71.2 ± 7.8 and 169.4 ± 51.6 nm. Each group of NdAuNP was referred as NdAuNP 30 nm, 70 nm and 170 nm for convenience. (b) UV−Vis absorption spectra showed characteristic peaks corresponding to surface plasmon of gold nanoparticles, with red shift as the AuNP size increased from 30 to 170 nm (c) SEM and TEM (inset) images were obtained. The scale bar of TEM images is 50 nm. (d) The zeta potential measurement revealed that introduction of more amine groups gives less negative charges on the nanoparticle surface. (e) P2T assay was performed to determine number of amine groups introduced on the AuNP surface after amination process by using $0–3\%$ of NH_4OH. Number of amine groups increased as the concentration of NH_4OH was raised as expected.

P2T was detected from dAuNPs. The degree of amination increased as the concentration of added ammonium hydroxide solution increased ranging from 0 to 3%. Taken together, primary amine groups could be introduced onto the surface of NdAuNP with control over number of amines.

Next, to examine thermal stability of the prepared AuNPs, three sets of AuNPs—NdAuNPs, dAuNPs, and conventional citrate stabilized AuNPs (cit-AuNPs) with respective sizes were prepared in distilled water. The prepared AuNPs were heated in a thermocycler at 100 °C for 48 h. Colloidal stability of the AuNPs was estimated by measuring UV−Vis absorption spectra at various time points because surface plasmon peak corresponding to each AuNP can be considered as an indicator of intact AuNPs. The UV−Vis spectra suggested that colloidal stability of NdAuNPs was maintained over 50% up to 24 (30 nm), 12 (70 nm), and 6 h (170 nm) at 100 °C

whereas cit-AuNP completely decomposed within a few hours (Figure S1). The graph of relative plasmon band intensities plotted as a function of incubation time in Figure S1d showed relationship between nanoparticle size and thermal stability. The result indicated that the colloidal stability of AuNPs was highly enhanced by dextran coating and even further improved by crosslinking and amination of surface-coated dextran. The smallest 30 nm NdAuNPs exhibited best colloidal stability at 100 °C.

The colloidal stability of each sized NdAuNPs, dAuNPs and cit-AuNPs was next determined in acidic/basic pH conditions and a couple of biological buffer solutions by measuring UV−Vis absorption spectra of the nanoparticle solutions for four days. All the NdAuNPs showed excellent stability in biological buffers, including phosphate-buffered saline (PBS, pH 7.2) and 2-(N-morpholino) ethanesulfonic acid (MES, pH 6.5), up to four days, whereas

cit-AuNPs flocculated in 1 or 2 days (Figure S2a,b). The results suggested that surface coating of AuNPs with dextran made the AuNPs more suitable for biological applications than cit-AuNPs by showing better stability in biological buffers. In highly acidic (pH 2) and basic (pH 12) conditions, about 80% of cit-AuNPs lost colloidal stability within 2 days. However, over 60% of 30 and 70 nm NdAuNPs remained well dispersed in pH 2 and 12 up to four days and 50% of 170 nm NdAuNPs showed good stability up to 1 day (Figure S2c,d). Overall, NdAuNPs showed good colloidal stability compared to cit-AuNPs, suggesting better suitability for various biological applications.

We next prepared fluorescent dye labeled NdAuNPs to facilitate fluorescent imaging of the nanoparticles under a conventional fluorescence microscope. N-hydroxysuccinimide (NHS) end modified cyanine 5.5 (Cy5.5) was conjugated to primary amine residues on the surface of NdAuNPs in aqueous solution. After purification using size exclusion chromatography, the number of conjugated Cy5.5 fluorescent dye was revealed as 1.2 per NdAuNP by measuring UV−Vis absorption of the Cy5.5-conjugated NdAuNPs at 675 nm and calculating the concentration of Cy5.5 (extinction coefficient of Cy5.5, $\varepsilon_{Cy5.5, 675 nm} = 250,000 \text{ M}^{-1} \text{ cm}^{-1}$). Subsequently, doxorubicin (Dox, also known as hydroxydaunorubicin which is popularly used

anti-cancer compound) was conjugated to Cy5.5−NdAuNPs by using a homo-bifunctional, amine-reactive NHS ended crosslinking reagent, di(N-succinimidyl) glutarate linker (DSG). We calculated number of conjugated Dox per nanoparticle-based on UV−Vis absorption of Dox-conjugated AuNPs obtained at 480 nm (extinction coefficient of Dox, $\varepsilon_{Dox, 480 nm} = 11,500 \text{ M}^{-1} \text{ cm}^{-1}$, Figure S3). We found that 1.2 ± 0.2 of Dox per nanoparticle was conjugated in all cases with high reproducibility. Basically, the degree of Dox conjugation was quantitatively controllable by adjusting the amount of the DSG linker and Dox during conjugation reactions. We found that the colloidal stability of the Dox-NdAuNPs decreased as the number of Dox on the NdAuNPs surface increased probably due to its hydrophobicity and thus, we decided to use ∼1 Dox-conjugated NdAuNPs for further characterization and all the experiments in this study to prevent unwanted agglomeration in biological conditions.

To evaluate cytotoxicity and Dox delivery efficiency of the prepared NdAuNPs, 30, 70, and 170 nm Cy5.5 labeled NdAuNPs (Cy5.5−NdAuNP) and doxorubicin conjugated Cy5.5−NdAuNPs (Dox−Cy5.5−NdAuNP, ∼1 Dox per particle) were treated to HeLa cells and cell viability was measured after 12 h of incubation by MTT assay. Cy5.5−NdAuNPs (30, 70, 170 nm) themselves showed very low cytotoxicity in HeLa cells by showing ∼80% of cell viability
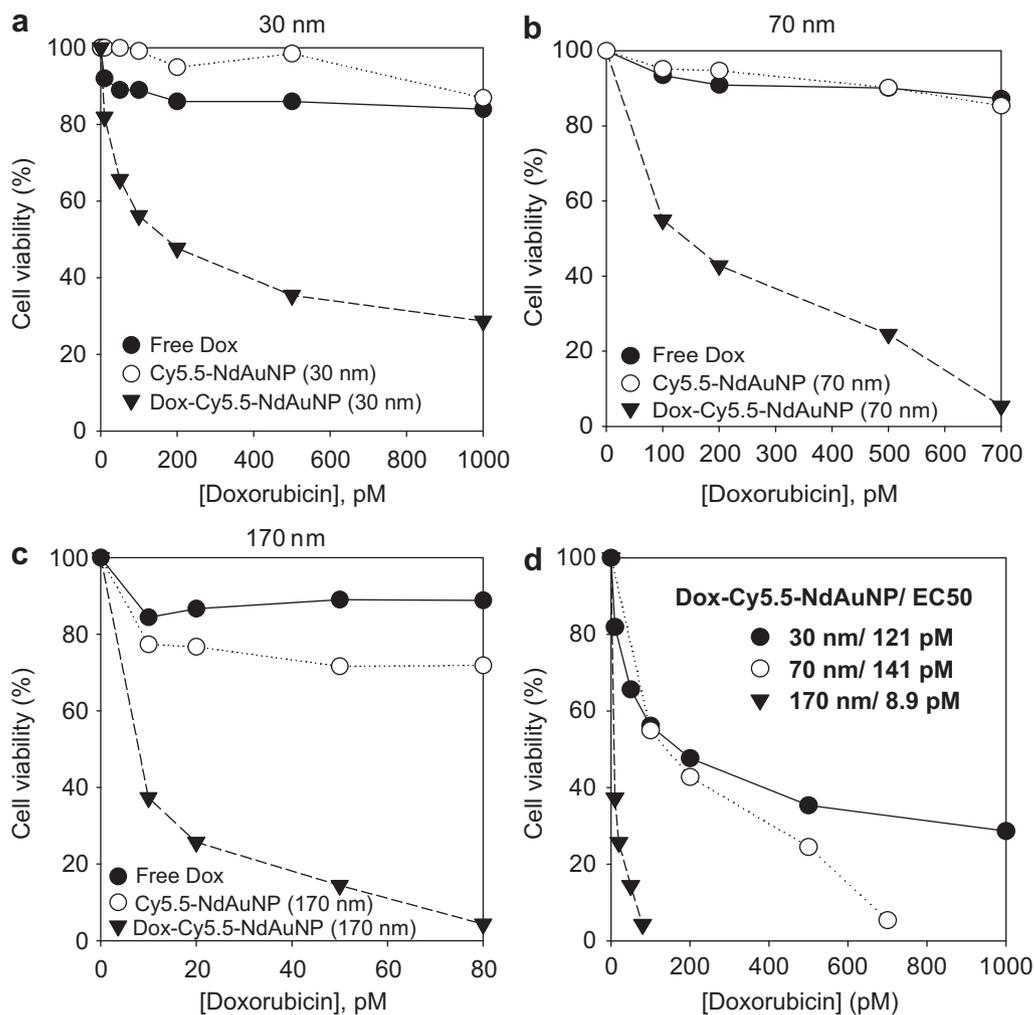

Fig. 2. Viability of the HeLa cells treated with free doxorubicin, and 30, 70, and 170 nm Cy5.5−NdAuNPs and Dox-Cy5.5−NdAuNPs was measured by MTT assay. The viability data for the cells treated with 30 (a), 70 (b), and 170 (c) nm nanoparticles were shown and their merged data were plotted in (d). Compared to the previously reported EC50 of free doxorubicin towards HeLa cells (0.6–1.4 μM), the EC50 of Dox−Cy5.5−NdAuNPs were substantially lower ranging from 141 to 8.9 pM, indicating that 7.1×10^3–1.1×10^5 times less doxorubicin is required to achieve same efficacy as free doxorubicin if the dextran-coated AuNPs were used for delivery vehicle. We calculated concentration of the surface conjugated Dox based on extinction coefficient of Dox. In case of non-Dox loaded Cy5.5−NdAuNPs, we used equal concentration of the particles with Dox−Cy5.5−NdAuNPs.

at the highest concentration we used (1 nm, Fig. 2). To investigate efficiency for Dox delivery, we compared viabilities of HeLa cells after treated with Dox–Cy5.5–NdAuNPs and free Dox for 12 h. Surprisingly, Dox–Cy5.5–NdAuNPs exhibited high cytotoxicity at extremely low concentrations by showing EC50 of 121, 141 and 9 pM with 30, 70 and 170 nm particles, respectively. Considering that the reported EC50 of free Dox for HeLa cells is in the range of 0.6–1.4 μM, the picomolar range of EC50 of Dox–Cy5.5–NdAuNPs is substantially low and can be considered as remarkable improvement of efficiency of Dox as an anti-cancer drug. If the EC50 of free Dox is estimated as 1 μM, 30, 70, and 170 nm Dox–Cy5.5–NdAuNPs showed $8.3' 10^3$, $7.1' 10^3$ and $1.1' 10^5$ times less EC50 than free Dox. We merged cell viability data of Dox–Cy5.5–NdAuNPs of 30, 70 and 170 nm and plotted as a function of Dox concentration to compare the efficacy in accordance with nanoparticle size (Fig. 2d). The plot revealed the amazingly eminent efficacy of 170 nm NdAuNPs as a Dox delivery vehicle, which is much bigger than nuclear pores and thus, almost impossible to enter across the nuclear membrane. Therefore, Dox might be released from big gold cores and diffused into nucleus to exhibit this high efficacy. Under the circumstances, Dox would be localized in nuclei unlike Cy5.5 that might be present both in cytoplasm and nuclei without any preference.

To investigate the intracellular localization of Dox and Cy5.5, we next obtained fluorescence micrographs of HeLa cells treated with three sets of Dox–Cy5.5–NdAuNPs with different sizes (∼83 pM) and free Dox (∼83 pM) for 12 h (Fig. 3). To distinguish, nuclei were stained with DAPI, showing blue fluorescence in the images. Fluorescence corresponding to Cy5.5 and Dox was color-coded as red and green, respectively. In the cells treated with free Dox, fluorescence signal corresponding to Dox was hardly observed. The HeLa cells treated with 30 nm Dox–Cy5.5–NdAuNP presented intense fluorescence signals corresponding to Cy5.5 and Dox with quite even spatial distribution throughout cytoplasm and nucleus, indicating that the particles might enter into nucleus and Dox could be active in nucleus while maintaining conjugation with the nanoparticles since Cy5.5 and Dox are highly co-localized both in cytoplasm and nucleus. However, this high co-localization was not observed in the cells treated with 70 nm Dox–Cy5.5–NdAuNPs and relatively more intense Dox fluorescence was observed inside nucleus compared to Cy5.5. It seemed that Dox was accumulated in nucleus due to intercalation with DNA, whereas Cy5.5 distributed evenly in cytoplasm and nucleus. The accumulation of Dox in nucleus was also observed in the cells treated with 170 nm Dox–Cy5.5–NdAuNPs. The nanoparticles larger than 70 nm in diameter were considered too large to enter into cell nucleus. Therefore,
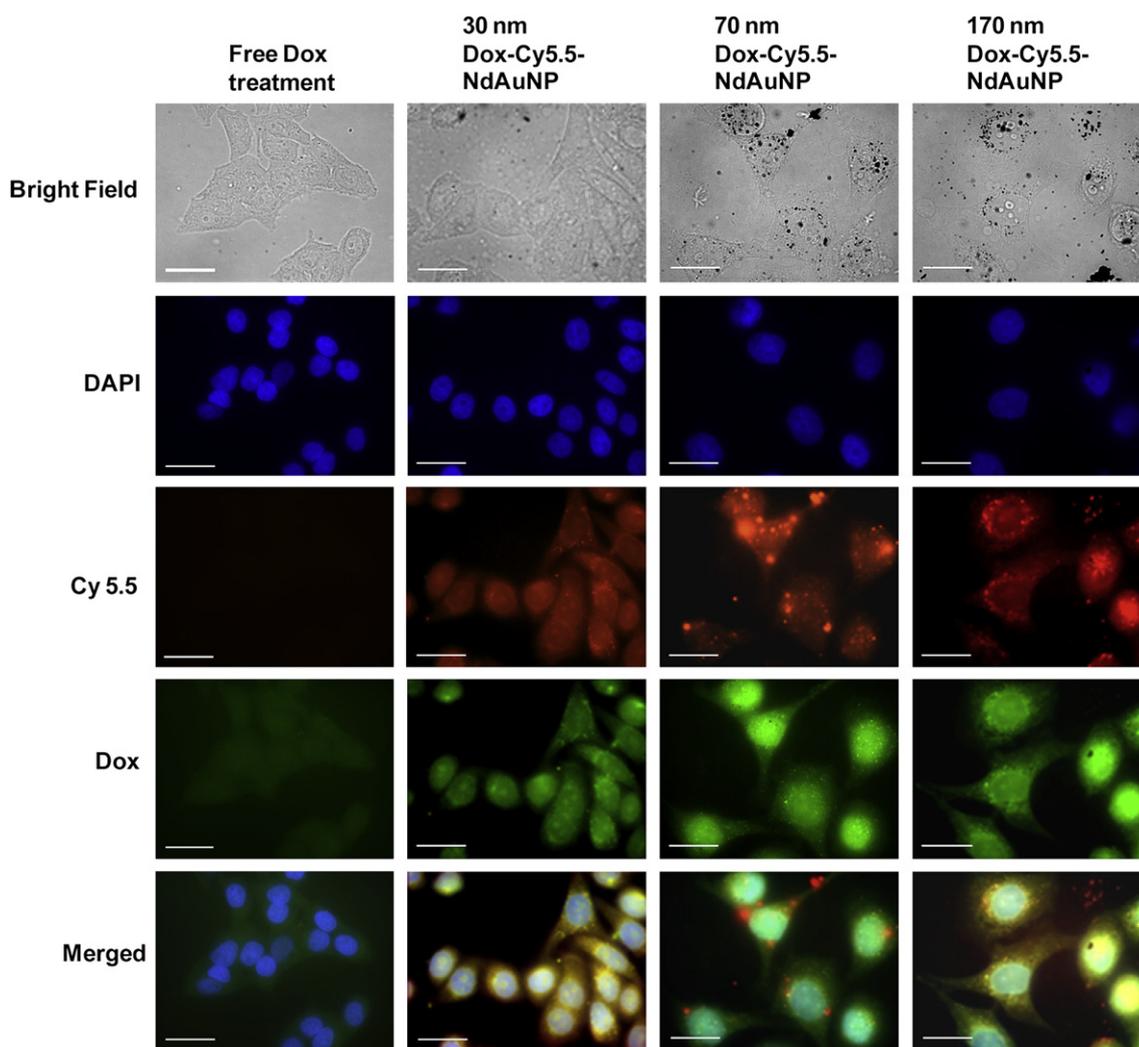

Fig. 3. Fluorescence microscopic images of HeLa cells treated with 30, 70, and 170 nm Dox–Cy5.5–NdAuNPs. Cells were treated with Dox-conjugated nanoparticles for 12 h before imaging. Fluorescence intensity corresponding to doxorubicin was especially intense inside nuclei compared to cytoplasm in the cells treated with 70 nm and 170 nm Dox–Cy5.5–NdAuNPs, whereas the fluorescence signal was relatively homogenous throughout the nuclei and cytoplasm in case of 30 nm Dox–Cy5.5–NdAuNP. The scale bar is 20 μm.
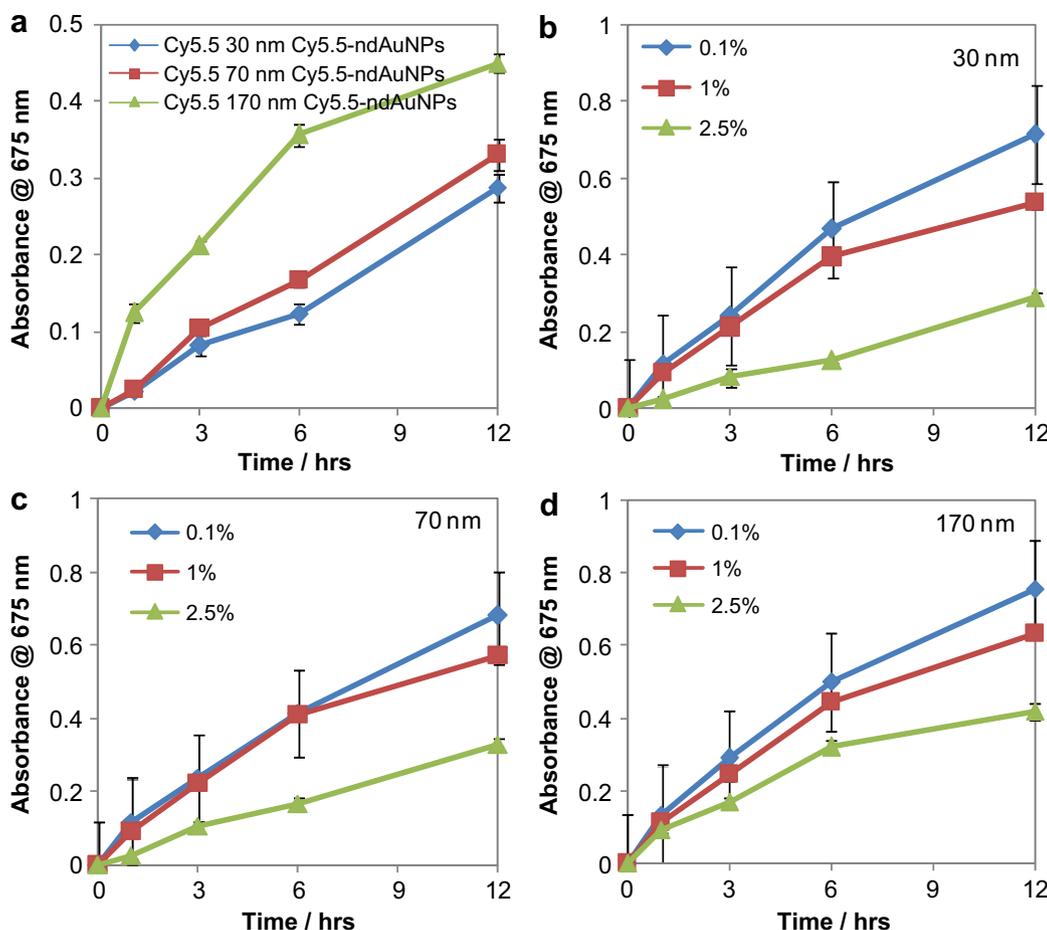
Fig. 4. Release profile of Cy5.5 from Cy5.5–NdAuNPs by spontaneous degradation of dextran coating. (a) Degradation of dextran coating of AuNPs (30, 70, 170 nm) was monitored by measuring absorbance of released Cy5.5 at 675 nm. AuNPs of 170 nm showed the fastest release of Cy5.5 probably due to higher surface area and less crosslinking compared to smaller particles. (b) (c) (d) Three AuNPs (30, 70, 170 nm for (b), (c), (d), respectively) with different degree of crosslinking (0.1, 1, 2.5 v/v%) were prepared and tested for Cy5.5 release kinetics. As expected, more dextran crosslinking slowed down degradation of dextran shell, which resulted in slower release of Cy5.5 chemically conjugated to outer shell of NdAuNPs in all the AuNPs tested.

in case of 70 and 170 nm particles, Dox and Cy5.5 would be released from gold cores due to the breakage of dextran coating, and then, both small molecules freely diffused throughout the whole intracellular area, resulting in the intracellular accumulation of Dox due to its intercalation with double stranded DNA. In case of 30 nm particles, it seemed that diffusion of the Dox-particle complex was faster than degradation of dextran and subsequent release of Dox [43–45]. However, EC50 of 30 nm particle was comparable to that of 70 nm Dox–Cy5.5–NdAuNPs, probably because 30 nm particles can diffuse more freely into nucleus for Dox–DNA interaction than 70 nm particles even though slower dextran degradation was expected. Smaller EC50 value of 170 nm particles than 70 or 30 nm particles might be due to faster degradation of dextran coating.

Next, we investigated degradation kinetics of dextran shell from the AuNPs by measuring absorbance of the released Cy5.5 overtime while incubating the Cy5.5–NdAuNPs in PBS at room temperature (Fig. 4). Cy5.5 was released faster from bigger particles probably due to faster hydrolysis of dextran shell induced by larger surface area and lower degree of crosslinking (Fig. 4a). To reveal the relationship of degradation kinetics with degree of crosslinking of dextran shells, we measured the release kinetics of Cy5.5 from Cy5.5–NdAuNPs with different sizes (30, 70, 170 nm) and three different degree of dextran crosslinking (0.1, 1, 2.5%). Cy5.5 was released faster from the particles with lower percentage of dextran

crosslinking in all the AuNPs with three different sizes as expected (Fig. 4b, c, d). Taken together, release kinetics of therapeutics from the delivery cargo dAuNP could be precisely tuned by controlling degree of crosslinking and size of AuNPs.

4. Conclusion

In summary, 30–170 nm sized dextran-coated AuNPs were synthesized and applied to efficient nuclear delivery of Dox, where the surface conjugated Dox was released apart from the AuNP cores after the Dox-conjugated AuNPs were internalized inside cells, by the degradation of dextran coating in the cell cytoplasm. Such a strategy for the delivery of Dox based on the degradable biopolymer coated AuNPs substantially increased efficiency of Dox as an anti-cancer agent by showing up to 1.1×10^5 times higher cytotoxicity compared to free Dox. Even though the size of the nanoparticle complex was much larger than that of nuclear pores (~30–40 nm), the released Dox from the AuNP cores was able to freely diffuse and accumulated inside nucleus without necessity of NLS and thus, giving much improved cytotoxicity. In addition, the dextran-coated AuNPs maintained colloidal stability in biological buffers and even under harsh conditions such as high temperature and extreme pHs, which makes the nanoparticles readily applicable for a wide range of biological applications.

Acknowledgments

Appendix A. Supplementary data

Supplementary data related to this article can be found at http://dx.doi.org/10.1016/j.biomaterials.2013.01.076.

References

[1] De M, Ghosh PS, Rotello VM. Applications of nanoparticles in biology. Adv Mater 2008;20:4225–41.
[2] Berry CC, Curtis ASG. Functionalisation of magnetic nanoparticles for applications in biomedicine. J Phys D: Appl Phys 2003;36:R198–206.
[3] Gupta AK, Gupta M. Synthesis and surface engineering of iron oxide nanoparticles for biomedical applications. Biomaterials 2005;26:3995–4021.
[4] Bruchez M, Moronne M, Gin P, Weiss S, Alivisatos AP. Semiconductor nanocrystals as fluorescent biological labels. Science 1998;281:2013–6.
[5] Slowing II, Trewyn BG, Lin VS. Mesoporous silica nanoparticles for intracellular delivery of membrane-impermeable proteins. Adv Funct Mater 2007;17:8845–9.
[6] Marinakos SM, Anderson MF, Ryan JA, Martin LD, Feldheim DL. Encapsulation, permeability, and cellular uptake characteristics of hollow nanometer-sized conductive polymer capsules. J Phys Chem B 2001;105:8872–6.
[7] Liu J, Zhang Q, Remsen EE, Wooley KL. Nanostructured materials designed for cell binding and transduction. Biomacromolecules 2001;2:362–8.
[8] Davda J, Labhasetwar V. Characterization of nanoparticle uptake by endothelial cells. Int J Pharm 2002;233:51–9.
[9] Patra HK, Banerjee S, Chaudhuri U, Lahiri P, Dasgupta AK. Cell selective response to gold nanoparticles. Nanomedicine: Nanotech Biol Med 2007;3:111–9.
[10] Schiffelers RM, Ansari A, Xu J, Zhou Q, Tang Q, Storm G, et al. Cancer siRNA therapy by tumor selective delivery with ligand-targeted sterically stabilized nanoparticle. Nucleic Acids Res 2004;32:e149.
[11] Cho EC, Xie J, Wurm PA, Xia Y. Understanding the role of surface charges in cellular adsorption versus internalization by selectively removing gold nanoparticles on the cell surface with a I2/KI etchant. Nano Lett 2009;9:1080–4.
[12] Zhang LW, Monteiro-Riviere NA. Mechanisms of quantum dot nanoparticle cellular uptake. Toxicol Sci 2009;110:138–55.
[13] Panyam J, Labhasetsar V. Biodegradable nanoparticles for drug and gene delivery to cells and tissue. Adv Drug Deliv Rev 2003;55:329–47.
[14] Asati A, Santra S, Kaittanis C, Perez JM. Surface-charge-dependent cell localization and cytotoxicity of cerium oxide nanoparticles. ACS Nano 2010;4:5321–31.
[15] Tkachenko AG, Xie H, Coleman D, Glomm W, Ryan J, Anderson MF, et al. Multifunctional gold nanoparticle-peptide complexes for nuclear targeting. J Am Chem Soc 2003;125:4700–1.
[16] Kubitscheck U, Grunwald D, Hoekstra A, Rohleder D, Kues T, Siebrasse JP, et al. Nuclear transport of single molecules: dwell times at the nuclear pore complex. J Cell Biol 2005;168:233–43.
[17] Mizutani H, Tada-Oikawa S, Hiraku Y, Kojima M, Kawanishi S. Mechanism of apoptosis induced by doxorubicin through the generation of hydrogen peroxide. Life Sci 2005;76:1439–53.
[18] Pan L, He Q, Lui J, Chen Y, Ma M, Zhang L, et al. Nuclear-targeted drug delivery of TAT peptide-conjugated monodisperse mesoporous silica nanoparticles. J Am Chem Soc 2012;134:5722–5.
[19] Niikura K, Sekiguchi S, Nishio T, Masuda T, Akita H, Matsuo Y, et al. Oligosaccharide-mediated nuclear transport of nanoparticles. Chembiochem 2008;9:2623–7.
[20] Eguchi A, Furusawa H, Yamamoto A, Akuta T, Hasegawa M, Okahata Y, et al. Optimization of nuclear localization signal for nuclear transport of DNA-encapsulating particles. J Control Release 2005;104:507–19.
[21] Liu JN, Bu W, Pan LM, Zhang S, Chen F, Zhou L, et al. Simultaneous nuclear imaging and intranuclear drug delivery by nuclear-targeted multifunctional upconversion nanoprobes. Biomaterials 2012;33:7282–90.
[22] Porkka K, Laakkonen P, Hoffman JA, Bernasconi M, Ruoslahti E. A fragment of the HMGN2 protein homes to the nuclei of tumor cells and tumor endothelial cells in vivo. Proc Natl Acad Sci U S A 2002;99:7444–9.
[23] Tiwari PM, Vig K, Dennis VA, Singh SR. Functionalized gold nanoparticles and their biomedical applications. Nanomaterials 2011;1:31–63.
[24] Giljohann DA, Seferos DS, Daniel WL, Massich MD, Patel PC, Mirkin CA. Goldnanoparticles for biology and medicine. Angew Chem Int Ed Engl 2010;49:3280–94.
[25] Dubertret B, Calame M, Libchaber AJ. Single-mismatch detection using gold-quenched fluorescent oligonucleotides. Nat Biotechnol 2001;19:365–70.
[26] Dulkeith E, Ringler M, Klar TA, Feldmann J. Gold nanoparticles quench fluorescence by phase induced radiative rate suppression. Nano Lett 2005;5:585–9.
[27] Okamoto T, Yamaguchi I. Optical absorption study of the surface plasmon resonance in gold nanoparticles immobilized onto a gold substrate by self-assembly technique. J Phys Chem B 2003;107:10321–4.
[28] Mey JD, Lambert AM, Bajer AS, Moeremans M, Brabander MD. Visualization of microtubules in interphase and mitotic plant cells of haemanthus endosperm with the immune-gold staining method. Proc Natl Acad Sci U S A 1982;79:1898–902.
[29] Felsenfeld DP, Choquet D, Sheetz MP. Ligand binding regulates the directed movement of beta1 integrin on fibroblasts. Nature 1996;383:438–40.
[30] Faulk WP, Taylor GM. Communication to the editors: an immunocolloid method for the electron microscope. Immunochemistry 1971;8:1081–3.
[31] Kim S, Lim YT, Soltesz EG, Grand AMD, Lee J, Dor A, et al. Near-infrared fluorescent type II quantum dots for sentinel lymph node mapping. Nat Biotechnol 2004;22:93–7.
[32] Salem AK, Searson PC, Leong KW. Multifunctional nanorods for gene delivery. Nat Mater 2003;2:668–71.
[33] Ghosh P, Han G, De M, Kim CK, Rotello VM. Gold nanoparticles in delivery applications. Adv Drug Deliv Rev 2008;60:1307–15.
[34] Huang XH, Jain PK, El-Sayed H, El-Sayed MA. Determination of the minimum temperature required for selective photothermal destruction of cancer cells with the use of immunotargeted gold nanoparticles. Photochem Photobiol 2006;82:412–7.
[35] Hamad-Schifferli K, Schwartz JJ, Santos AT, Zhang S, Jacobson JM. Remote electronic control of DNA hybridization through inductive coupling to an attached metal nanocrytal antenna. Nature 2002;415:152–5.
[36] Li YL, Zhu L, Liu Z, Cheng R, Meng F, Cui JH, et al. Reversibly stabilized multifunctional dextran nanoparticles efficiently deliver doxorubicin into the nuclei of cancer cells. Angew Chem Int Ed Engl 2009;48:9914–8.
[37] Duong HTT, Hughes F, Sagnella S, Kavallaris M, Macmillan A, Whan R, et al. Functionalizing biodegradable dextran scaffolds using living radical polymerization: new versatile nanoparticles for the delivery of therapeutic molecules. Mol Pharm 2012;9:3046–61.
[38] Arbab AS, Wilson LB, Ashari P, Jordan EK, Lewis BK, Frank JA. A model of lysosomal metabolism of dextran coated superparamegnetic iron oxide (SPION) nanoparticles: implications for cellular magnetic resonance imaging. NMR Biomed 2005;18:383–9.
[39] Jordan A, Wust P, Scholz R, Tesche B, Fahling H, Mitrovics T, et al. Cellular uptake of magnetic fluid particles and their effects on human adenocarcinoma cells exposed to AC magnetic fields in vitro. Int J Hyperthermia 1996;12:705–22.
[40] Jang H, Kim YK, Ryoo SR, Kim MH, Min DH. Facile synthesis of robust and biocompatible gold nanoparticles. Chem Commun 2010;46:583–5.
[41] Zhao M, Kircher MF, Josephson L, Weissleder R. Differential conjugation of tat peptide to superparamagnetic nanoparticles and its effect on cellular uptake. Bioconjug Chem 2002;13:840–4.
[42] Ngo TT. A simple spectrophotometric determination of solid supported amino groups. J Biochem Biophys Methods 1986;12:349–54.
[43] Broaders KE, Cohen JA, Beaudette TT, Bachelder EM, Frechet JM. Acetalated dextran is a chemically and biologically tunable material for particulate immunotherapy. Proc Natl Acad Sci U S A 2009;106:5497–502.
[44] Van Dijk-Wolthuis WNE, Hoogeboom JAM, Van Steenbergen MJ, Tsang SKY, Hennink WE. Degradation and release behavior of bextran-based hydrogels. Macromolecules 1997;30:4639–45.
[45] Cohen JA, Beaudette TT, Cohen JL, Broaders KE, Bachelder EM, Frechet JM. Acetal-modified dextran microparticles with controlled degradation kinetics and surface functionality for gene delivery in phagocytic and non-phagocytic cells. Adv Mater 2010;22:3593–7.